Plasticity Decay and Attenuated Recovery (PDAR): A Hybrid Dynamical Model for the Historical Accessibility of Evolutionary Space

Hidetomo Maruta
Independent Researcher

Abstract

The evolutionary history of life is marked by a pronounced temporal asymmetry: an early, disproportionate generation of major morphological novelty, followed by extensive taxonomic diversification that does not appear to be accompanied by comparable expansion of morphological disparity. This paper develops a minimal hybrid dynamical model, termed Plasticity Decay and Attenuated Recovery (PDAR), that treats this asymmetry not as a static limit on evolution but as a consequence of a dynamic feedback between adaptation and the accessibility of future evolutionary states. Three state variables are introduced: accessible evolutionary potential $P(t)$, selective/optimization state $S(t)$, and accumulated structural and developmental constraint $C(t)$. Continuous adaptive optimization is coupled to a monotonically accumulating constraint that lowers a state-dependent capacity bound $K(C)$, while catastrophic events (e.g. mass extinctions) are represented as discrete impulses that release selection pressure without instantaneously erasing accumulated constraint. We derive conditions for forward invariance of the admissible state space, prove that unbounded constraint accumulation forces evolutionary potential toward zero in the limit, and show numerically that repeated catastrophic release combined with persistent constraint generates a characteristic attenuated sawtooth trajectory. The model yields falsifiable, quantitative predictions distinguishing it from established mechanisms such as ecological saturation, niche limitation, and extinction selectivity. A preliminary empirical assessment using three independent, publicly archived paleontological datasets finds heterogeneous post-extinction disparity responses rather than a uniform pattern, consistent with the model's rejection of a universal "extinction $\Rightarrow$ expansion" rule, while the distinctive historically-conditioned attenuation mechanism itself remains to be directly tested.

1 Introduction

The evolutionary history of life is characterized not only by an increase in taxonomic diversity, but also by a pronounced temporal asymmetry in the generation of morphological novelty. The diversification of metazoans during the early Phanerozoic, particularly during the Cambrian radiation, represents one of the most conspicuous episodes of morphological innovation in the history of life [1, 2]. A large fraction of the major architectural organizations of extant metazoans emerged within a relatively short geological interval, motivating extensive debate about the mechanisms responsible for the early establishment of animal body plans [3, 4].

Importantly, the subsequent history of animal life does not exhibit a simple continuation of this early expansion of morphological disparity. Taxonomic diversity has repeatedly increased following major extinction events, and adaptive radiations have generated enormous numbers of species and genera. Nevertheless, the emergence of fundamentally new anatomical organizations appears to have become comparatively restricted. This motivates a conceptual separation between taxonomic diversity (the number, richness, or relative abundance of recognized evolutionary lineages) and morphological disparity (the distribution and extent of morphological variation within a defined morphospace) [3, 4, 15].

We refer to a lineage's capacity to generate and tolerate alternative developmental configurations from which novel phenotypic structures may emerge as its morphological evolutionary potential, or morphological innovability. The central hypothesis developed here is that this capacity is not necessarily constant through evolutionary time: adaptive optimization may itself alter the internal architecture of developmental systems in ways that reduce future evolutionary freedom,

$$\begin{gathered}\text{Adaptive Optimization} \longrightarrow \text{Structural Integration} \longrightarrow \\ \text{Developmental Constraint} \longrightarrow \text{Reduced Evolutionary Potential.}\end{gathered} \tag{1}$$

This relationship is not proposed as a claim that every adaptive change reduces evolvability; rather, it concerns the cumulative effect of repeated optimization and integration over long evolutionary timescales.

This motivates three interrelated hypotheses, developed mathematically in Section 3. **Hypothesis 1 (Constraint Accumulation)**: repeated adaptive optimization increases the degree of structural coupling and developmental interdependence within a lineage. **Hypothesis 2 (Capacity Decay)**: the maximum evolutionary potential available to a lineage decreases as developmental constraint accumulates. **Hypothesis 3 (Attenuated Recovery)**: catastrophic events temporarily reduce environmental selection and release previously suppressed phenotypic variation, but do not erase the structural developmental constraint that has accumulated in surviving lineages.

The resulting mathematical model is termed the **Plasticity Decay and Attenuated Recovery (PDAR)** model. PDAR is intended as a mechanistic hypothesis about the long-term dynamics of evolvability, not as a replacement for natural selection, mutation, genetic drift, or developmental biology; rather, it introduces an additional, state-dependent mechanism operating on macroevolutionary timescales. Accordingly, the central empirical prediction is not simply that evolutionary change declines through time. Instead, the model predicts a specific combination of observations: taxonomic diversity may continue to increase, adaptive radiation may repeatedly occur after extinction, yet the capacity for major morphological innovation should exhibit a long-term decline or saturation.

2 Biological Motivation

PDAR abstracts several biological phenomena, operating at different levels of organization, into a single dynamical framework. None of these phenomena individually demonstrates PDAR; together they motivate treating structural and developmental integration as a cumulative, historically evolving state.

Genome architecture. Genome streamlining — the loss of substantial fractions of the genome under specialization, particularly in parasitic and symbiotic lineages — illustrates how specialization can reduce the repertoire of genetic functions accessible to a lineage [7, 8]. **Gene duplication and subfunctionalization.** The Duplication–Degeneration–Complementation (DDC) model [9] describes how gene duplication can lead to functional partitioning between paralogs, so that the ancestral function is reconstituted only by the joint action of both copies — a process that can increase functional and regulatory interdependence even as it stabilizes duplicated genes and creates new evolutionary potential. **Robustness and evolvability.** Genetic variation is not equivalent to phenotypically accessible variation; robust systems can harbor phenotypically silent genetic variation, and the relationship between robustness and evolvability is not universally antagonistic [10, 11]. **Developmental integration.** Increasing integration among genes, regulatory elements, and developmental processes can stabilize development while simultaneously increasing the number of interdependencies that must remain consistent under further change [20].

Together, these processes motivate a hierarchical abstraction,

$$\text{Genomic Architecture} \rightarrow \text{Regulatory Interdependence} \rightarrow \text{Developmental Integration} \rightarrow C(t), \tag{2}$$

where $C(t)$ is a single latent state variable representing accumulated structural and developmental constraint, and a historical asymmetry related to, but weaker than, Dollo's Law [21, 22]: environmental conditions can change rapidly, but the developmental and structural architecture accumulated prior to an environmental transition is not necessarily erased on the same timescale.

3 Mathematical Model

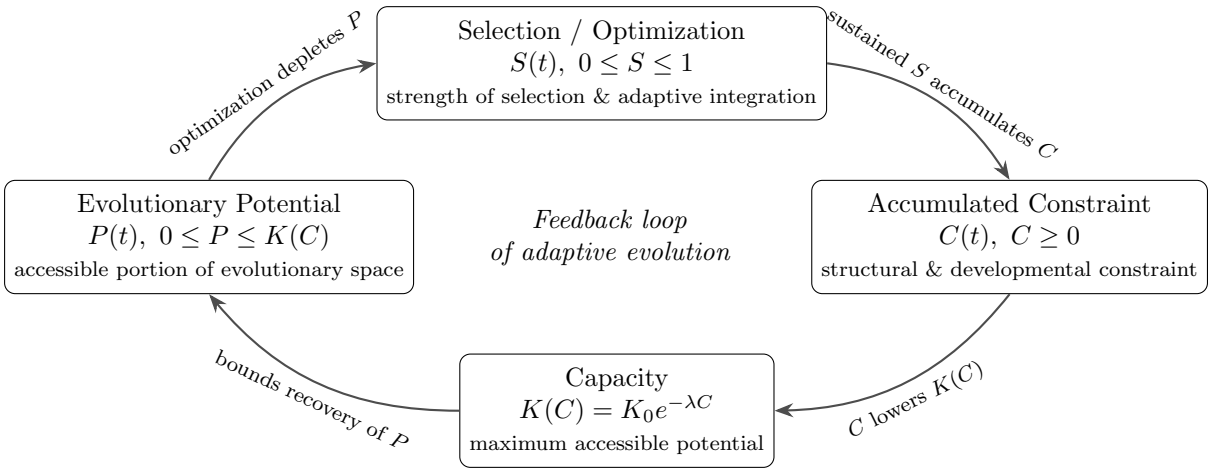

Figure 1: The PDAR feedback structure. Sustained selection/optimization S depletes accessible evolutionary potential P while accumulating structural constraint C; C lowers the capacity bound $K(C)$, which in turn limits how far P can recover.

Figure 1 summarizes the feedback structure formalized below.

3.1 State variables

PDAR introduces three state variables:

$$P(t) = \text{accessible evolutionary potential}, \qquad S(t) = \text{selective/optimization state}, \tag{3}$$

$$C(t) = \text{accumulated structural and developmental constraint}. \tag{4}$$

Crucially, $P(t)$ is not genetic diversity or mutation rate; it is the phenotypically accessible portion of evolutionary space,

$$P(t) \neq \text{genetic diversity}, \qquad P(t) = \text{accessible evolutionary potential}. \tag{5}$$

$S(t) \in [0, 1]$ represents the strength of selection/adaptive integration to the current environment, and $C(t)$ is a composite state variable representing the accumulated structural dependencies described in Section 2.

3.2 Capacity function

The maximum evolutionary potential available to a lineage is assumed to decay with accumulated constraint:

$$K(C) = K_0 e^{-\lambda C}, \qquad K_0 > 0,\ \lambda > 0, \tag{6}$$

so that $dK/dC = -\lambda K(C) < 0$. The exponential form is not claimed to be empirically unique; it is the simplest positive, monotonic, memory-dependent function satisfying $K(0) = K_0$ and $K'(C) < 0$. The corresponding state constraint is $0 \le P(t) \le K(C(t))$.

3.3 Continuous-time dynamics

Between catastrophic events, the system evolves according to

$$\frac{dP}{dt} = \mu\sqrt{P}\left(1 - \frac{P}{K(C)}\right) - \alpha SP, \tag{7}$$

$$\frac{dS}{dt} = \beta S(1 - S), \tag{8}$$

$$\frac{dC}{dt} = \gamma\alpha SP, \tag{9}$$

with $\mu, \alpha, \beta, \gamma > 0$. The first term in Eq. (7) represents intrinsic recovery of accessible evolutionary potential toward the current capacity bound; the second term, $-\alpha SP$, represents depletion under sustained adaptive optimization. Equation (8) describes logistic approach of the selection/optimization state toward $S = 1$ absent disturbance. Equation (9) states that structural constraint accumulates whenever both selection and evolutionary exploration are simultaneously active; since $S, P \ge 0$, $C(t)$ is non-decreasing in continuous time.

3.4 Hybrid dynamics: catastrophic impulses

A central feature of the PDAR model is the distinction between continuous evolutionary dynamics and rapid environmental perturbations such as mass extinction events [13, 14], represented here as an impulsive (hybrid) dynamical system [12]. At the k-th catastrophic event, $t = t_k$, the state jumps according to

$$S(t_k^+) = \rho_k S(t_k^-), \qquad 0 \le \rho_k \le 1, \tag{10}$$

$$P(t_k^+) = \min\Big\{K(C(t_k^-)),\ P(t_k^-) + \eta(1 - \rho_k)\big[K(C(t_k^-)) - P(t_k^-)\big]\Big\}, \tag{11}$$

$$C(t_k^+) = C(t_k^-). \tag{12}$$

Equation (12) encodes the central asymmetry of the model: environmental reset does not imply architectural reset,

$$\text{Environmental Reset} \neq \text{Evolutionary Architectural Reset}. \tag{13}$$

3.5 Invariance, monotonicity, and asymptotic decay

Let $\Omega = \{(P, S, C) : P \ge 0,\ 0 \le S \le 1,\ C \ge 0,\ P \le K(C)\}$. Setting $Q(t) = P(t) - K(C(t))$, differentiating along the boundary $P = K(C)$, and using Eqs. (7)–(9) gives

$$\left.\frac{dQ}{dt}\right|_{P=K} = \alpha SK\big(\lambda\gamma K - 1\big). \tag{14}$$

Hence a sufficient condition for forward invariance of Ω under the continuous dynamics is

$$\lambda\gamma K_0 \le 1. \tag{15}$$

The catastrophic map preserves Ω automatically, since Eq. (11) enforces $P(t_k^+) \leq K(C(t_k^-)) = K(C(t_k^+))$. Because $dC/dt \geq 0$ in continuous time and C is unchanged at jumps, $C(t)$ is non-decreasing overall; this is a modeling assumption representing timescale asymmetry, not a claim of literal irreversibility. Consequently $K(C(t))$ is non-increasing, and if $C(t) \to \infty$ then, by the squeeze theorem applied to $0 \leq P(t) \leq K(C(t)) \to 0$,

$$C(t) \to \infty \;\Rightarrow\; P(t) \to 0. \tag{16}$$

This conditional result is the strongest analytic consequence of the model; it is not a claim that biological evolution must terminate in finite time, only an asymptotic limit conditional on unbounded constraint accumulation.

3.6 Additional analytical properties

Several further properties follow directly from Eqs. (7)–(9) and clarify which qualitative features of PDAR are mathematical consequences of the stated assumptions rather than additional hypotheses. Between catastrophes, Eq. (8) is autonomous and logistic, with exact solution

$$S(t) = \frac{1}{1 + (S_0^{-1} - 1)e^{-\beta t}}, \qquad 0 < S_0 < 1, \tag{17}$$

so $S(t) \to 1$ monotonically on a timescale of order β^{-1}, independently of P and C.

For S and K treated as frozen parameters, setting $dP/dt = 0$ with $y = \sqrt{P}$ gives $(\mu/K)y^2 + \alpha S y - \mu = 0$, with positive root

$$y_q = \frac{-\alpha S K + \sqrt{\alpha^2 S^2 K^2 + 4\mu^2 K}}{2\mu}, \qquad P_q = y_q^2. \tag{18}$$

The transformed dynamics $dy/dt = f(y) = \frac{\mu}{2}(1 - y^2/K) - \frac{\alpha S}{2} y$ satisfy $f'(y) = -\mu y/K - \alpha S/2 < 0$ for $y > 0$, so P_q is locally asymptotically stable for fixed $S > 0, K > 0$; since the recovery term vanishes at $P = K$ while depletion remains negative, $0 < P_q < K$ strictly. Implicit differentiation of $F(P, S, K) = \mu\sqrt{P}(1 - P/K) - \alpha S P = 0$ at P_q gives

$$\frac{\partial P_q}{\partial S} < 0, \qquad \frac{\partial P_q}{\partial K} > 0, \tag{19}$$

so that, since $K(C) = K_0 e^{-\lambda C}$, $C \uparrow \Rightarrow K \downarrow \Rightarrow P_q \downarrow$ — a local, mathematical version of the central PDAR feedback (conditional on the base-model functional forms, not a claim about biological universality).

The catastrophe map also admits a direct gap-closing interpretation. Writing $K_k = K(C(t_k^-))$ and $G_k = K_k - P(t_k^-)$, whenever the minimum operator is inactive, Eq. (11) gives $P(t_k^+) - P(t_k^-) = \eta(1 - \rho_k)G_k$, equivalently

$$K_k - P(t_k^+) = \big[1 - \eta(1 - \rho_k)\big]\big(K_k - P(t_k^-)\big), \tag{20}$$

so a non-saturating catastrophe closes a fixed fraction $\eta(1 - \rho_k)$ of the currently available gap, never an absolute amount independent of history. Finally, if two states share the same instantaneous S but $C_A > C_B$, then $K(C_A) < K(C_B)$ and, under the quasi-equilibrium approximation, $P_q(S, C_A) < P_q(S, C_B)$: identical contemporary conditions need not yield identical accessible potential when historical constraint differs, formalizing the path-dependence discussed qualitatively above.

4 Numerical Results

4.1 Baseline simulation

A representative baseline parameter set, satisfying the invariance condition (15) ($\lambda\gamma K_0 = 0.02 \leq 1$), is

$$K_0 = 1,\ \lambda = 0.1,\ \mu = 0.2,\ \alpha = 0.3,\ \beta = 0.5,\ \gamma = 0.2,\ \eta = 1.0,\ \rho = 0.2, \tag{21}$$

with $P(0) = 0.8$, $S(0) = 0.2$, $C(0) = 0$, and catastrophic events at $t_k = 20k$, $k = 1, \ldots, 8$. Table 1 summarizes the resulting trajectory at each event.

Accumulated constraint rises from $C \approx 0.38$ after the first interval to $C \approx 2.82$ after eight intervals, while the evolutionary capacity $K(C)$ correspondingly declines from ≈ 0.96 to ≈ 0.75. Critically, the system does not exhibit simple monotonic loss of P: catastrophic events repeatedly restore part of the distance between P and its current capacity. Recovery instead occurs within a progressively contracting envelope,

$$K(C(t_{k+1})) \leq K(C(t_k)), \tag{22}$$

generating a characteristic **attenuated sawtooth trajectory**: repeated recovery and optimization cycles whose upper envelope steadily contracts (Figure 3).

Table 1: Representative baseline trajectory at catastrophic events.

t_k	P^-	S^-	C	P^+	S^+	$K(C)$
20	0.254	1.000	0.381	0.821	0.200	0.963
40	0.250	1.000	0.757	0.792	0.200	0.927
60	0.246	1.000	1.123	0.764	0.200	0.894
80	0.242	1.000	1.479	0.738	0.200	0.863
100	0.238	1.000	1.827	0.714	0.200	0.833
120	0.234	1.000	2.166	0.691	0.200	0.805
140	0.230	1.000	2.496	0.669	0.200	0.779
160	0.227	1.000	2.819	0.649	0.200	0.754

4.2 Numerical verification of the analytical results

The baseline trajectory was checked directly against the analytical properties of Section 3.6. **(i) Moving boundary**: $Q(t) = P(t) - K(C(t))$ remains ≤ 0 throughout, consistent with $\lambda\gamma K_0 = 0.02 \leq 1$. **(ii) Logistic convergence**: with $S(0) = 0.2$, $\beta = 0.5$, the exact solution gives $S^- \approx 0.9998$ by $t = 20$, matching the numerical trajectory and confirming that the repeated sawtooth is driven by the prescribed hybrid reset mechanism rather than numerical artifact. **(iii) Quasi-equilibrium tracking**: at $t = 20$ ($S \approx 0.9998$, $K = 0.963$), Eq. (18) gives $P_q \approx 0.246$ against the simulated $P^- = 0.254$; at $t = 160$ ($K = 0.754$), $P_q \approx 0.222$ against $P^- = 0.227$ — close agreement, with the small positive gap consistent with finite-time relaxation toward a slowly-drifting target. **(iv) Recovery-gap ratio**: defining $R_k = [P(t_k^+) - P(t_k^-)]/[K(C(t_k^-)) - P(t_k^-)]$, the baseline gives $R_1 \approx 0.567/0.709 \approx 0.80$ and $R_8 \approx 0.422/0.527 \approx 0.80$, both matching $\eta(1-\rho) = 0.8$ exactly as predicted — confirming that attenuation arises from the shrinking gap G_k under a fixed reset fraction, not from any drift in η or ρ. **(v) Envelope versus peaks**: $K(C(t_k))$ is guaranteed non-increasing (0.963→0.754 in the baseline); the individual post-catastrophe values $P(t_k^+)$ also decline here, but this is a property of the chosen parameter regime rather than a theorem, since the model only guarantees monotonicity of the envelope itself. These checks confirm that the attenuated-sawtooth pattern is a structural consequence of Eqs. (7)–(12), not an artifact of a particular plot; they establish internal mathematical consistency, not empirical validity.

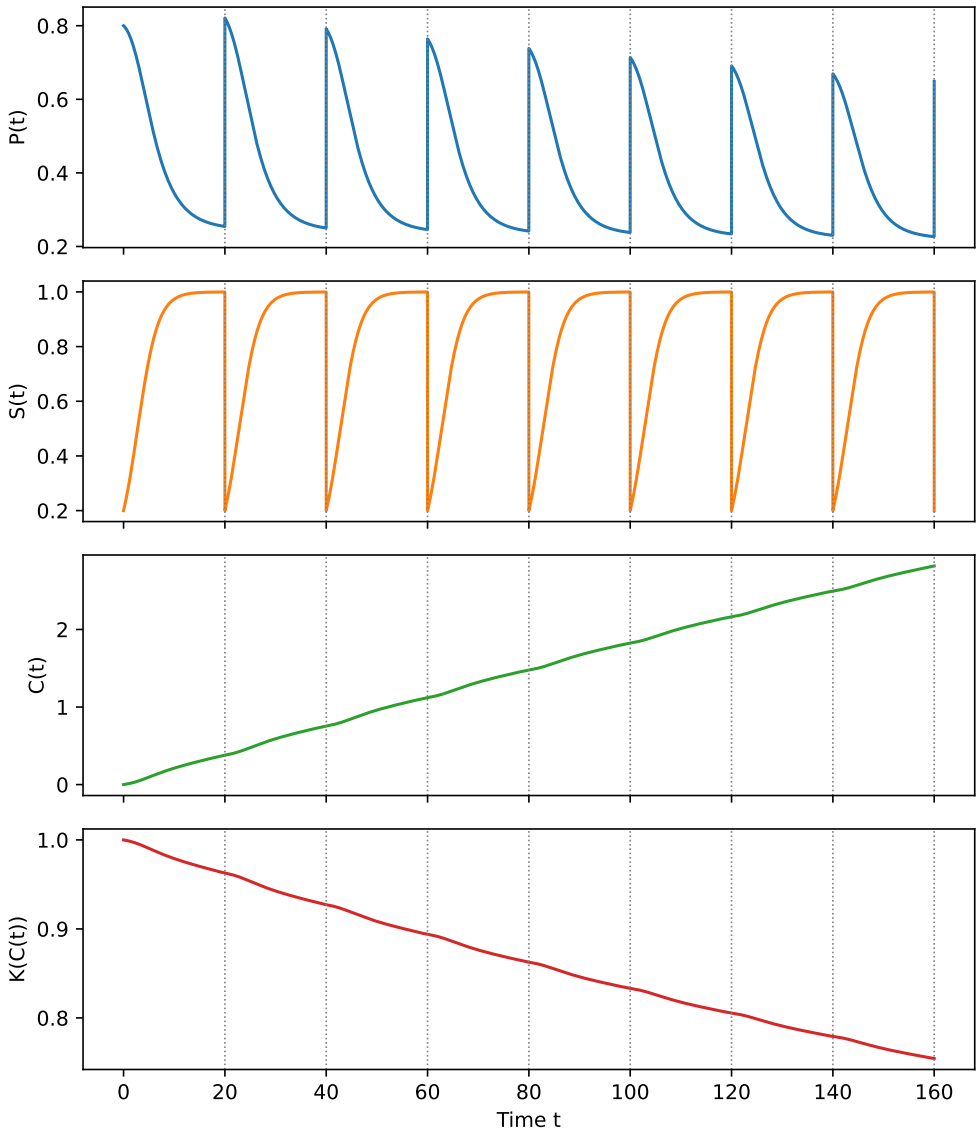

Figure 2: Numerical simulation of the PDAR model under the baseline parameter set of Eq. (21), showing $P(t)$, $S(t)$, $C(t)$, and $K(C(t))$ across eight catastrophic events (dotted vertical lines).

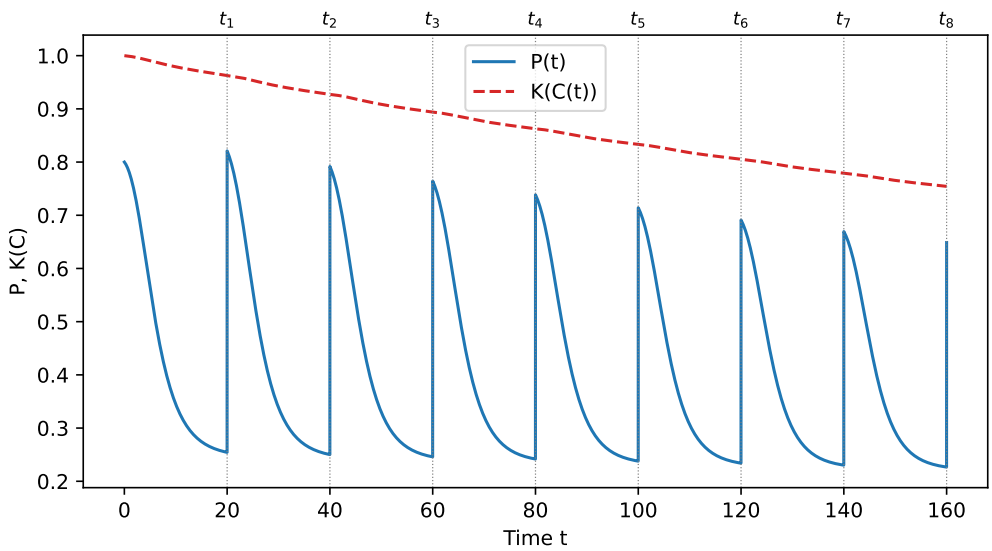

Figure 3: The attenuated sawtooth trajectory: $P(t)$ (solid) repeatedly recovers toward the capacity bound $K(C(t))$ (dashed) after each catastrophic event $t_1, \ldots, t_8$, but the bound itself contracts as constraint accumulates.

4.3 Parameter sensitivity

Table 2 summarizes the qualitative role of each parameter. The constraint-sensitivity parameter λ and the recovery parameter μ play structurally distinct roles: μ governs the rate at which P approaches its bound, whereas λ (together with C) governs the size of the accessible envelope itself — a highly evolvable system (μ large) can still be constrained by a sufficiently reduced capacity function. The catastrophic-release parameters η and ρ jointly determine the effective release amplitude $\eta(1-\rho)$, but even maximal release cannot push P beyond $K(C)$:

$$\text{Stronger Ecological Release} \not\Rightarrow \text{Unlimited Morphological Innovation.} \tag{23}$$

The interval between catastrophic events, Δt_{cat}, also matters: longer intervals allow S to approach 1 and sustain optimization for longer, increasing $\int \gamma\alpha S(t)P(t)\,dt$ and hence the constraint accumulated per cycle.

Table 2: Qualitative sensitivity of the PDAR dynamics.

Parameter	Principal dynamical effect
λ	Sensitivity of capacity to accumulated constraint; larger λ produces faster contraction of $K(C)$.
μ	Recovery rate of P toward the current capacity.
α	Coupling between selection/optimization and depletion of P; accelerates both P-depletion and C-accumulation.
β	Recovery rate of S following release.
γ	Conversion of optimization into accumulated constraint.
η	Magnitude of catastrophic release.
ρ	Fraction of selection retained after catastrophe (smaller ρ = stronger release).

4.4 Observational extension: disparity and diversity

To connect the latent variable P to observable macroevolutionary patterns, we introduce an observational layer. Morphological disparity $D(t)$ and taxonomic diversity $N(t)$ are represented schematically as

$$\frac{dD}{dt} = \delta P \left(1 - \frac{D}{D_{\max}}\right) - \epsilon D, \tag{24}$$

$$\frac{dN}{dt} = r(S)N \left(1 - \frac{N}{N_{\max}}\right) - m(t)N, \tag{25}$$

where δ is the rate of morphological innovation, ϵ is disparity erosion, $r(S)$ is ecologically-driven taxonomic diversification, and $m(t)$ is extinction pressure. These are observational extensions, not additional core assumptions. Because D is driven by P while N is driven largely by S, the model permits $\Delta N > 0$ while $\Delta D \ll \Delta N$ whenever accumulated constraint has already reduced $K(C)$ — i.e., taxonomic radiation need not imply proportional morphological expansion.

4.5 Hierarchical diversification: major versus minor innovation

The distinction between diversity and disparity introduced above can be sharpened by separating evolutionary change into two tiers: local diversification within an existing developmental framework, and innovation that reorganizes that framework itself. Denoting the occurrence rate of the latter by $\nu_{\text{major}}(t)$ and the former by $\nu_{\text{minor}}(t)$, a natural observational hypothesis is

$$\nu_{\text{major}}(t) \approx a\,K(C(t)), \qquad \nu_{\text{minor}}(t) \approx r(S(t)) + b\,K(C(t)), \qquad a, b > 0, \tag{26}$$

so that the rate of major innovation tracks the shrinking capacity bound, while ecologically-driven local diversification can persist even as ν_{major} declines (Figure 4). As with the observational extensions above, ν_{major} and ν_{minor} are not state variables derived directly from Eqs. (7)–(9), but a hypothesized observational construct for distinguishing "large-scale innovation" from "local diversification" empirically.

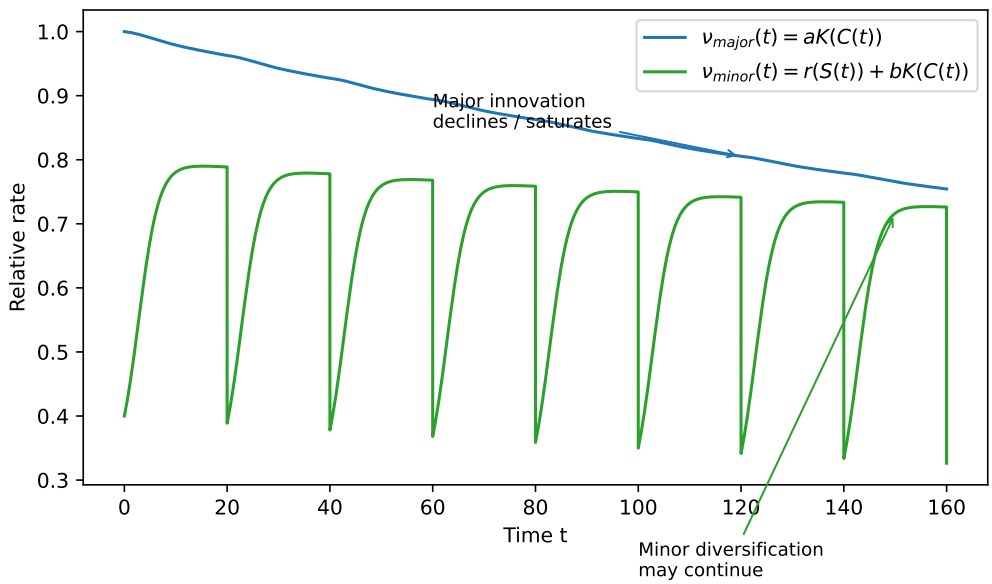

Figure 4: Schematic hierarchical diversification. The rate of major innovation $\nu_{\text{major}}(t)$ tracks the declining capacity bound, while locally-driven minor diversification $\nu_{\text{minor}}(t)$ can continue to increase over the same interval.

5 Testable Predictions

The model generates several falsifiable predictions, summarized in Table 3 at the level of mechanism, empirical observable, and predicted pattern.

Table 3: PDAR from the standpoint of empirical verification: model mechanism, corresponding observable, and predicted pattern.

Model mechanism	Empirical observable	Predicted pattern
Constraint accumulates, $dC/dt = \gamma\alpha SP \geq 0$	Developmental/genomic integration	Long-term increase
Capacity $K(C)$ declines, $K(C) = K_0 e^{-\lambda C}$	Disparity / morphospace accessibility	Declining recovery magnitude of major disparity
Catastrophe induces partial recovery, $P(t_k^+) > P(t_k^-)$	Post-extinction disparity	Transient increase
Recovery is incomplete, $P(t_k^+) \leq K(C(t_k^-))$	Recovery amplitude A_k	Long-term attenuation (decay)

In prose, (1) **Diminishing morphological recovery**: comparable ecological releases should show declining magnitude of recovery through evolutionary history, $K(C(t_{k+1})) \leq K(C(t_k))$. (2) **Disparity–diversity decoupling**: post-catastrophic radiations should not necessarily produce proportional increases in disparity, consistent with evidence that clades often attain peak morphological disparity early in their history [15, 3, 4]. (3) **Historical asymmetry**: lineages with different integration histories should show different accessible capacities even under similar current environments, consistent with the broader role of historical contingency in evolution [16]. (4) **Dependence on catastrophe interval**: longer intervals between disturbances, which permit more sustained optimization, should be associated with greater capacity contraction. (5) **Persistent architectural memory**: because $C(t_k^+) = C(t_k^-)$, the evolutionary response following release should retain detectable signatures of prior developmental or genomic integration.

The model is falsifiable in the sense of Popper [17]: if repeated, comparable ecological releases consistently show no reduction in subsequent morphological accessibility, the central capacity-decay hypothesis is weakened; if $C(t_k^+) = C(t_k^-)$ is repeatedly violated at the relevant timescale, that assumption requires revision; and if disparity and diversity consistently increase in close proportion, the predicted decoupling receives no support. Critically, PDAR is not falsified merely by individual lineages showing dramatic post-catastrophe innovation; the relevant test is whether the capacity for repeated recovery shows systematic historical attenuation after controlling for ecological opportunity.

5.1 Operationalization of P and C

The principal empirical challenge for PDAR is that $P(t)$ and $C(t)$ are latent theoretical states rather than directly observable biological quantities. Each should therefore be operationalized through multiple measurable indicators and estimated within a latent-variable framework.

For C, candidate proxies include developmental gene-regulatory-network (GRN) connectivity, pleiotropic coupling among genes and developmental traits, loss or partitioning of functional redundancy, and reduced modular independence of developmental programs; Hox-associated developmental processes provide an interpretable example of strong developmental coupling. These indicators should not be treated as interchangeable measurements of C: exploratory dimensional reduction (e.g. PCA) followed by confirmatory factor analysis or structural equation

modeling (SEM) can be used to estimate a latent constraint score $\hat{C}$ while representing measurement error. For P, candidate proxies include the locally accessible volume of morphospace estimated using geometric morphometrics, together with phylogenetically corrected evolutionary variance and repeated entry into previously sparsely occupied regions of phenotype space; variance and accessible state-space volume are complementary rather than identical quantities. Schematically,

$$\text{genomic/developmental indicators} \to \hat{C}, \tag{27}$$

$$\text{morphometric/phylogenetic indicators} \to \hat{P} \to \text{disparity and innovation.} \tag{28}$$

The criterion is predictive validity: $\hat{C}$ should predict subsequent reductions in accessible morphospace or recovery capacity, while $\hat{P}$ should predict major morphological innovation beyond mutation rate or taxonomic diversity alone. Alternative measurement models should be compared rather than assuming that any single proxy is the true state variable.

5.2 Parameter estimation and identifiability

The parameters of PDAR should be treated as estimable quantities rather than merely illustrative constants. Because the model is hybrid, estimation should combine continuous trajectories with discrete pre-/post-catastrophe observations. The recovery parameter μ can be estimated from the rate at which $\hat{P}$ approaches its contemporaneous capacity after perturbation; α from depletion under sustained selection; β from recovery of S after release; γ from the association between sustained optimization and subsequent increases in $\hat{C}$; and λ from the relationship between $\hat{C}$ and the upper envelope of accessible potential. The catastrophe parameters ρ and η can be estimated from the immediate change in the selection-related state and the fraction of the remaining capacity gap closed,

$$R_k = \frac{P(t_k^+) - P(t_k^-)}{K(C(t_k^-)) - P(t_k^-)} = \eta(1 - \rho_k), \tag{29}$$

which separates catastrophe-specific release from the historical capacity gap; repeated events across lineages can test whether attenuation arises from shrinking capacity, changing release strength, or both.

A single lineage or sparse time series will generally not identify all parameters reliably: μ and α may trade off, while λ and γ can both influence long-term contraction. Empirical estimation should therefore use hierarchical likelihood or Bayesian state-space methods, repeated perturbations, and independent measurements of developmental integration, reporting parameter-recovery simulations, profile likelihoods or posterior correlations, and out-of-sample prediction. The parameter set used in Section 4 is a demonstration of dynamical behavior, not an empirical estimate; future empirical work should report uncertainty intervals and compare PDAR with reduced models having constant K, non-accumulating C, or catastrophe-induced changes in both S and C.

5.3 Innovation-rate observation model

PDAR distinguishes latent capacity for major morphological innovation from the observed occurrence rate of evolutionary novelties; innovation rate should therefore be formulated as an observation model rather than identified directly with P,

$$\nu_{\text{major}}(t) = f\big(P(t), S(t), E(t)\big), \tag{30}$$

where $E(t)$ denotes ecological opportunity and other external factors. The present framework uses the first-order approximation $\nu_{\text{major}}(t) \approx aK(C(t))$ introduced in Section 4.5, while minor

diversification may additionally depend on ecological release through $r(S)$; this proportional form should be tested rather than assumed. Operational definitions of ν_{major} may include the rate of entry into previously sparsely occupied morphospace, statistically significant movement into new regions of phylogenetically corrected morphometric space, or the occurrence of qualitatively novel anatomical configurations, distinguished from ordinary phenotypic variance and species richness:

$$\hat{C} \to \hat{K} \to \text{accessible morphospace} \to \text{major-innovation rate}. \tag{31}$$

Ecological opportunity, extinction selectivity, clade age, and sampling intensity should enter as covariates or competing explanatory variables; support for PDAR is strongest if historical $\hat{C}$ predicts future major-innovation capacity after these factors are controlled.

5.4 Empirical tests that could falsify PDAR

Building on the falsifiability criteria stated above, five specific tests operationalize where the model could fail. **Test 1 (constraint accumulation)**: if developmental/genomic integration does not increase systematically with cumulative adaptive specialization, or independent integration measures fail to predict subsequent accessibility of phenotypic variation, the proposed C-dynamics are weakened. **Test 2 (capacity decay)**: if lineages with substantially different historical integration show no difference in subsequent accessible morphospace after controlling for ecology, clade age, phylogeny, sampling, and extinction history, the central $K(C)$ relation is weakened. **Test 3 (attenuated recovery)**: if repeated, comparable ecological releases produce recovery amplitudes that do not decline with prior constraint, or ecological opportunity alone explains recovery equally well, the distinctive PDAR prediction loses support. **Test 4 (architectural memory)**: if catastrophic or environmental release repeatedly resets developmental integration on the same timescale on which selection is released, the assumption $C(t_k^+) = C(t_k^-)$ must be rejected or reformulated. **Test 5 (diversity–disparity relation)**: if taxonomic diversification after ecological release consistently produces proportional expansion of major morphological disparity independent of historical constraint, the proposed separation between local diversification and major innovation is not supported. As emphasized above, a single lineage with spectacular post-extinction innovation does not falsify PDAR; the critical test is systematic historical attenuation across comparable perturbations after ecological opportunity and extinction selectivity are controlled.

5.5 Comparative method as the primary empirical strategy

Taken together, Sections 5.1–5.4 point to a comparative rather than single-lineage empirical strategy. A single temporal trajectory cannot readily distinguish accumulated constraint from environmental change, ecological saturation, sampling effects, or changing extinction intensity, whereas

$$\begin{gathered}\text{Comparable Ecological Opportunity} + \text{Different Historical Constraint} \\ \Rightarrow \text{Different Major Morphological Recovery}\end{gathered} \tag{32}$$

is directly testable across lineages. Sister or closely related lineages provide a stronger quasi-controlled comparison when they share ecological opportunity but differ in developmental or structural histories. The ideal design combines the comparative phylogenetic analysis, morphometric analysis, developmental/genomic data, and pre-/post-extinction comparisons introduced above: (i) comparative phylogenetic analysis testing whether lineages with different developmental/structural integration show different subsequent disparity given comparable ecological opportunity, controlling for phylogeny, generation time, and extinction history; (ii) morphometric analysis using geometric morphometrics to estimate $D(t)$ separately from $N(t)$, directly

testing for decoupling; (iii) developmental–genomic data combined via the latent-variable approach of Section 5.1; and (iv) pre-/post-extinction comparisons, the most direct natural experiments, comparing lineages with similar ecological release but different historical constraint. The strongest evidence would be a repeated cross-lineage relationship in which an independently estimated $\hat{C}$ predicts both lower accessible morphospace and smaller recovery amplitude following comparable ecological release.

6 Preliminary Empirical Assessment

This section assesses whether publicly available paleobiological datasets show patterns compatible with the qualitative predictions of PDAR. The assessment is explicitly preliminary: the latent states $P(t)$ and $C(t)$ are not directly observed, and the datasets used do not permit a complete parameterized test of the hybrid model. The strategy therefore distinguishes observed morphological disparity $D(t)$ and taxonomic diversity $N(t)$ from the latent state $P(t)$, and asks whether their qualitative behavior around real extinction events is consistent with the model rather than attempting to estimate its parameters.

6.1 Data sources

Three published, publicly archived morphometric datasets spanning independent clades and extinction events were used. **Actinopterygians across the Permian–Triassic**: body-shape landmark data from Smithwick & Stubbs [24] (Dryad 10.5061/dryad.3vs6b). **Sharks across the Cretaceous–Paleogene**: 597 dental landmark configurations for Lamniformes and Carcharhiniformes from Bazzi et al. [25] (Dryad 10.5061/dryad.k30c2n0). **Strophomenid brachiopods across the Late Ordovician extinction**: morphospace and occurrence data from Sclafani et al. [26] (Dryad 10.5061/dryad.4bp82rc), supplemented by Paleobiology Database occurrence records. Disparity was estimated using multivariate variance and centroid distance, with rarefaction and bootstrap resampling used throughout to reduce sensitivity to unequal sample sizes; because these measures are not interchangeable, agreement across metrics is preferable to reliance on any single statistic. For the shark dataset, the present reanalysis performed an independent Generalized Procrustes and principal-component analysis (the first four PCs explaining $\approx 91.3\%$ of variance) rather than reproducing the original semilandmark-sliding pipeline exactly, and should be regarded as an independent exploratory analysis rather than an exact replication.

6.2 Permian–Triassic actinopterygians

Total variance in body shape across the principal Permian–Triassic bins was: Late Permian 0.03024, Induan 0.03252, Olenekian 0.02997, Early Triassic 0.03213, Anisian 0.02481, Ladinian 0.02618. The Late Permian-to-Induan (immediate post-extinction) difference was +0.00236, with a rarefied bootstrap 95% interval of $[-0.00685, 0.01206]$ — statistically compatible with no immediate change. A broader regression across 10-Myr bins likewise showed no significant monotonic trend ($r = -0.188$, $p = 0.603$). This null result does not by itself support a decline in $P(t)$, since $D(t)$ is only an observational proxy; it does, however, weigh against the simpler expectation that mass extinction must automatically produce a large morphospace expansion, consistent with PDAR's distinction between ecological release and architectural capacity.

6.3 Cretaceous–Paleogene sharks

The two shark clades showed markedly different responses. Lamniformes disparity was essentially unchanged across the boundary (0.06993 in the Maastrichtian vs. 0.06943 in the

Danian–Selandian; rarefied difference ≈ 0.000014, 95% interval $[-0.01548, 0.01571]$). Carcharhiniformes, by contrast, declined from 0.05746 to 0.03980 (rarefied difference -0.01876, 95% interval $[-0.02427, -0.01356]$, excluding zero). This heterogeneity argues against a universal "extinction $\Rightarrow$ morphospace expansion" rule, but the Carcharhiniform decline cannot be attributed uniquely to PDAR: extinction selectivity, trophic restructuring, and prey availability are equally plausible contributors. The relevant PDAR-specific test is not whether any single lineage expands after extinction, but whether comparable ecological release yields systematically smaller recovery where historical constraint is greater — a comparative question this dataset alone cannot resolve.

6.4 Diversity–disparity decoupling in Strophomenida

The Strophomenida dataset (Paleobiology Database snapshot, ≈16,800 occurrences, 363 genera) shows a pronounced Ordovician peak in occurrences and taxon counts followed by a long decline through the Silurian–Devonian, alongside the morphospace and recovery dynamics reported by Sclafani et al. [26] following the Late Ordovician extinction. These raw patterns are qualitatively compatible with a diversity–disparity decoupling framework, but collection intensity, geographic coverage, and preservation vary substantially through this interval; coverage-standardized joint analysis of $N(t)$ and $D(t)$, rather than raw counts, is needed before drawing strong macroevolutionary conclusions.

6.5 A cautionary note on constraint and evolutionary rate

A small supplementary comparison (eight *Anolis* species) tested whether an independent proxy for phenotypic integration predicts terminal-branch morphological rate. The predicted negative relationship was not supported ($r \approx 0.19$, $p \approx 0.66$ and $r \approx -0.08$, $p \approx 0.85$ across two marker sets). Given $n = 8$, this comparison has very limited statistical power and should not be read as evidence against PDAR; it is reported only to illustrate a conceptual refinement it motivates: on the short population-level timescales separating radiations of this kind from mass-extinction cycles, accumulated integration may be expected to constrain the directions and covariance structure of accessible variation well before it detectably reduces aggregate morphological rate. Distinguishing these two signatures requires axis-specific evolutionary-rate and covariance analyses that are beyond the scope of the present preliminary assessment.

6.6 Proxy-based estimation of accumulated constraint

Because $C(t)$ is a composite latent state, it is unlikely to be captured by any single observable measure; multiple partial proxies may instead be combined to estimate its historical variation,

$$\hat{C}(t) = F\big(I_{\text{net}}, H_{\text{dep}}, M_{\text{coup}}, I_{\text{sub}}, I_{\text{para}}, \dots\big), \tag{33}$$

where the components are candidate indicators rather than alternative definitions of C. Candidates include developmental gene-regulatory-network integration (using resources such as STRING [27] and BioGRID [28], e.g. mean degree or network density among conserved developmental modules), dependence on highly connected hub genes, reduced modularity (increasing cross-module connectivity), a DDC-based subfunctionalization index following gene duplication [9], and the degree of functional interdependence among retained paralogs. Cross-species comparisons using these indicators must control for annotation completeness and network-reconstruction differences. A hierarchical or latent-variable model combining such indicators could estimate $\hat{C}(t)$ and test whether higher inferred constraint predicts lower accessible morphospace or smaller recovery amplitude following comparable ecological opportunity — the complementary, upstream half of the empirical pathway genomic/developmental integration

$\to \hat{C} \to \hat{K} \to$ accessible morphospace $\to$ recovery, whose downstream half is examined in the fossil analyses above.

These genomic proxies target the upstream mechanisms of constraint accumulation directly — (1) loss of redundant genetic information and (2) increasing regulatory/developmental complexity that makes further modification harder — but require network- or annotation-scale data that are unavailable for essentially all fossil taxa, since genomic information does not survive in deep time. A complementary strategy is to test the downstream, phenotypic signature that these mechanisms are predicted to leave in the fossil record: if constraint accumulates at the genomic/developmental level, the morphospace realized by surviving lineages should become correspondingly more concentrated. This signature can be extracted as a size-zero proxy directly from the Procrustes-aligned landmark coordinates already used in Section 6, requiring no additional data collection. Let $X \in \mathbb{R}^{n\times p}$ be the GPA-aligned coordinate matrix (n specimens, p traits) for a given time bin, with covariance $\Sigma = \mathrm{Cov}(X)$ and eigenvalues $\lambda_i > \epsilon$ ($i = 1, \ldots, p'$). Define

$$\mathrm{ICV} = \frac{\sqrt{\mathrm{Var}(\lambda)}}{\mathrm{Mean}(\lambda)}, \qquad n_{\mathrm{eff}} = \frac{\left(\sum_i \lambda_i\right)^2}{\sum_i \lambda_i^2} \in [1, p'], \tag{34}$$

where n_{eff} is the participation ratio, an effective dimensionality of the occupied morphospace: it equals p' when variance is spread evenly across axes and approaches 1 as variance concentrates onto a single axis. ICV and n_{eff} are proposed here as exploratory candidate indicators, not as established measures of integration; PDAR predicts $C \uparrow \Rightarrow \mathrm{ICV} \uparrow, n_{\mathrm{eff}} \downarrow$, and this prediction, if borne out, would be sharper than one stated in terms of total disparity alone: because n_{eff} characterizes the shape of Σ rather than its trace, it could in principle decline even while total disparity $\mathrm{tr}(\Sigma)$ recovers after a catastrophe, offering one candidate explanation for diversity–disparity decoupling. It would also be more discriminating against simple ecological saturation, which has no obvious mechanism for producing a systematic decline in n_{eff}, though ecological saturation is a verbal model that makes no quantitative eigenvalue-spectrum prediction of its own, so this contrast should be read as a plausibility argument rather than a formally derived one. Combined with the literature-based developmental indicators N_{ct} (number of cell types) and H_{mult} (Hox cluster multiplicity), an exploratory composite index is

$$\hat{C}_{\mathrm{light}} = w_1 \log(1+\mathrm{ICV}) + w_2 \log(p'/n_{\mathrm{eff}}) + w_3 \log(N_{ct}) + w_4 H_{\mathrm{mult}}, \qquad w_i \geq 0,\ \sum_i w_i = 1. \tag{35}$$

Applying this to the actual Permian–Triassic actinopterygian PC scores analyzed above [24] (rarefied to a common $n = 26$ specimens per bin, $B = 2000$ bootstrap resamples) gives $n_{\mathrm{eff}} = 2.49\ [1.79, 3.59]$ for the Late Permian and $2.74\ [1.95, 3.85]$ for the Induan — essentially unchanged across the boundary itself (bootstrap difference $0.26\ [-1.13, 1.64]$), consistent with the null result already reported for total disparity. Across the full Late Permian–Ladinian sequence, however, n_{eff} shows a significant increasing trend with time ($r = 0.85$, $p = 0.03$; values $2.49 \to 2.74 \to 3.42 \to 3.32 \to 3.87 \to 3.69$), while ICV shows a non-significant decreasing trend ($r = -0.41$, $p = 0.42$) — the opposite direction from a naive reading of $C \uparrow \Rightarrow n_{\mathrm{eff}} \downarrow$. This is not a mismatch of level — the fossil-derived proxy is exactly the downstream observable the framework calls for, since the genomic mechanisms ((1),(2) above) cannot themselves be measured in deep time — but plausibly a mismatch of phase: the interval sampled is the post-extinction radiation itself, corresponding in the model to the catastrophic-release phase ($S \downarrow$, $P \uparrow$) rather than the subsequent sustained-optimization phase during which genomic-level constraint is predicted to accumulate, so an expanding effective morphospace dimension is plausible during release. We do not treat this as an ad hoc excuse, however: taken at face value, this single result, drawn from a phase the sharper prediction was not designed to address, can neither support nor refute PDAR on its own. The appropriate test of $C \uparrow \Rightarrow n_{\mathrm{eff}} \downarrow$ requires comparing n_{eff} across a sustained inter-catastrophe interval, or at its approach toward a subsequent capacity ceiling, rather than across a recovery window immediately following a mass extinction. We report this result, including the direction that runs counter to the naive prediction, rather than omitting it.

6.7 Status of the empirical evidence

Taken together, constraint accumulation has not been directly estimated; capacity decay has indirect and mixed support from the disparity record (heterogeneous rather than uniform post-extinction responses, and an increasing rather than decreasing effective morphospace dimension across the post-extinction radiation examined above); and attenuated recovery, while a sharply testable prediction, has not yet been demonstrated across repeated, quantitatively comparable extinction–recovery events. This preliminary assessment therefore neither confirms nor falsifies PDAR: it narrows the empirical question to a specific set of testable relationships, demonstrates that the required disparity, diversity, and integration measurements are obtainable from existing public data, and illustrates that testing these relationships can yield results running counter to a naive reading of the model, motivating the phase-dependent refinement noted above. The historically-conditioned attenuation mechanism that most distinguishes PDAR from alternative explanations remains untested.

7 Relation to Existing Evolutionary Concepts

PDAR is deliberately not presented as the discovery of developmental constraint, evolvability, canalization, robustness, Dollo's Law, adaptive radiation, or niche release. These are established concepts with substantial literatures, and each captures an important part of the biological background motivating the present model. The proposed novelty lies at a different level: PDAR integrates several established mechanisms into a single historical dynamical hypothesis concerning how the accessibility of future evolutionary states may change through time.

Developmental constraint [20] can describe why particular variants are difficult to produce; evolvability and robustness [10, 11] concern the capacity to generate heritable variation and the buffering of phenotypes under perturbation; canalization [5] describes stabilization of developmental outcomes; Dollo's principle [21, 22] captures historical asymmetry in evolutionary reversal; adaptive radiation [23] and niche release describe diversification following ecological opportunity. PDAR does not replace these concepts or claim that any one of them is insufficient on its own. Instead, it asks whether their interaction can be represented as a feedback process in which successful adaptation contributes, under specified conditions, to the accumulation of constraint, that accumulated constraint reduces accessible evolutionary capacity, and environmental release produces only partial recovery because historical constraint remains:

$$\text{Adaptation} \to C \uparrow \to K(C) \downarrow \to P_{\text{accessible}} \downarrow, \tag{36}$$

while catastrophic release is represented by

$$\text{Catastrophe} \to S \downarrow \to P \uparrow, \qquad C(t_k^+) = C(t_k^-). \tag{37}$$

The defining asymmetry is that the environmental or selective state can be reset rapidly, whereas the accumulated architectural state is retained on the modeled timescale. Thus, environmental reset does not imply evolutionary architectural reset. This distinction is the source of the attenuated-sawtooth behavior: repeated ecological release can reopen part of the currently accessible evolutionary space without restoring the historical capacity that has already been lost under the model assumptions.

In this sense, PDAR should be understood as a synthesis at the level of dynamical organization rather than a new name for any individual mechanism. Its mathematical contribution is to make the proposed feedback explicit through coupled state variables, a moving capacity boundary, and a hybrid catastrophe map. This formulation permits analytical statements and quantitative predictions that are not implied merely by listing the component concepts — for example, the conditional result that unbounded accumulation of C forces $K(C)$ and hence P toward zero, the prediction that comparable ecological releases can yield different recoveries in

lineages with different constraint histories, and the prediction that recovery amplitude depends on the remaining capacity gap.

The correspondence with established concepts can be summarized as follows. Several biological examples illustrate cases in which the qualitative pattern predicted by PDAR is realized, without individually demonstrating the model. Regressive evolution of eyes and pigmentation in cave-adapted *Astyanax mexicanus* [18] illustrates how developmental integration, not simple gene loss, can restructure a phenotype (but does not directly test $C(t_k^+) = C(t_k^-)$, since no catastrophic release is involved). The striking conservation of seven cervical vertebrae across nearly all mammals, despite extensive diversification elsewhere, has been linked to somitogenesis, Hox-mediated regionalization, and pleiotropy [19], illustrating $C \uparrow \Rightarrow$ (accessible phenotypic space)$\downarrow$ rather than absolute prohibition of change. Quantitative studies of Cambrian and post-Cambrian disparity likewise show that the timing and magnitude of morphological innovation is more complex than a simple "everything happened in the Cambrian" narrative [3, 4, 15], consistent with (but not requiring) an evolving capacity bound $K(C)$ rather than a fixed one.

Table 4: Correspondence between established evolutionary concepts and the PDAR framework.

Concept	Primary explanatory target	Position within PDAR
Developmental Constraint	Developmental limitation of variation	Biological basis contributing to the latent state $C(t)$
Evolvability	Capacity to generate and respond to evolutionary variation	Conceptual motivation for the accessible-potential state $P(t)$
Canalization	Stabilization/buffering of developmental outcomes	One possible biological route by which accessible phenotypic variation may be restricted; not identified with P or C
Robustness	Persistence of function under perturbation	Provides biological context for why genetic variation and accessible phenotypic variation need not coincide
Dollo's Principle	Historical asymmetry in evolutionary reversal	Related to persistence of $C(t)$, but weakened from absolute irreversibility to timescale-dependent historical asymmetry
Adaptive Radiation	Diversification following ecological release	Corresponds to the release component $S \downarrow \Rightarrow P \uparrow$, without requiring $K(C) \uparrow$
Niche Release	Increased ecological opportunity after environmental change	Provides a biological interpretation of changes in S, while PDAR predicts the response is conditioned by inherited C
Disparity–Diversity	Morphological vs. taxonomic diversification	Observation layer linking P to D and ecological diversification to N

Similarly, PDAR does not equate adaptive radiation with a restoration of the full evolutionary capacity of a lineage. In the model, ecological release lowers S and can increase P relative to its pre-release value, while C remains unchanged and $K(C)$ therefore remains historically con-

ditioned. Adaptive radiation and niche release are consequently compatible with PDAR rather than alternatives to it; the discriminating question is whether repeated releases of comparable ecological opportunity produce systematically different magnitudes of morphological recovery as a function of prior constraint.

The distinction is especially important for robustness, canalization, and evolvability. These concepts do not imply a universal one-directional relationship between buffering and future innovation; robustness can, for example, preserve cryptic genetic variation and thereby sometimes facilitate evolvability. PDAR therefore does not assume that every increase in robustness or canalization reduces evolutionary potential. Rather, the model treats persistent structural integration as one possible aggregate source of constraint and asks whether its historical accumulation produces the predicted reduction in accessible state space.

7.1 Alternative explanations and model limitations

Several established mechanisms can produce superficially similar patterns and must be distinguished empirically from PDAR rather than assumed away: ecological saturation ($N \to N_{\max}$, independent of $K(C)$); niche limitation / environmental stability, which produces stasis without necessarily implying $P \downarrow$; incomplete fossil sampling, which can make $D_{\text{observed}} \neq D_{\text{true}}$; extinction selectivity, in which selective (not random) extinction restructures surviving morphology independent of any change in evolutionary potential; and phylogenetic/developmental constraint specific to individual lineages, which PDAR treats as one biological source contributing to C rather than a competing explanation. The strongest empirical strategy is therefore comparative: lineages with comparable ecological opportunity but different historical constraint should show systematically different morphological recovery,

$$\begin{gathered}\text{Comparable Ecological Opportunity} + \text{Different Historical Constraint} \\ \Rightarrow \text{Different Morphological Recovery.}\end{gathered} \tag{38}$$

This is a substantially more discriminating test than asking merely whether disparity declines through time.

8 Discussion and Limitations

The model has clear limitations. First, $K(C) = K_0 e^{-\lambda C}$ is one functional form among several plausible alternatives; exponential decay is not claimed to be universal. Second, C collapses multiple distinct biological sources of constraint (genetic, developmental, morphological, ecological, behavioral) into a single scalar state variable. Third, population structure, spatial structure, gene flow, and interspecific interactions are not explicitly modeled. Fourth, as scaffolding and exaptation illustrate, existing structure can sometimes generate new evolutionary potential rather than only constraining it, so $K(C)$ may not be monotonically decreasing in all lineages or all timescales; a generalized model with a constraint-relaxation term, $dC/dt = \gamma\alpha SP - \kappa C$ with $\kappa \geq 0$, recovers the base model at $\kappa = 0$ and is a natural direction for extension, though the invariance and asymptotic results of Section 3.5 do not automatically transfer to $\kappa > 0$ without additional conditions. Fifth, no single empirical measure of P or C yet exists; connecting the abstract state variables to measurable quantities (genetic redundancy, network connectivity, phenotype-space volume, disparity, innovation rate) is a priority for future work.

9 Conclusion

PDAR treats evolution not as a process of fitness maximization within a fixed space of possibilities, but as a dynamical process unfolding within a possibility space that itself deforms

historically. Its central proposition is that adaptation does not only solve present problems, but can also change the set of solutions possible in the future. Repeated cycles of optimization, constraint accumulation, catastrophic release, and partial recovery generate an attenuated sawtooth: not simple stasis, and not unbounded innovation, but a historically contingent narrowing of the accessible space within which diversification continues. The model does not claim that evolution must inevitably cease; its falsifiable claim is more limited — that conditions exist under which the accumulation of adaptation systematically narrows future evolutionary potential, an effect that can manifest, over the long term, as a decline in the rate of major morphological innovation even as taxonomic diversity continues to grow.

References

[1] Gould, S. J. (1989). *Wonderful Life: The Burgess Shale and the Nature of History*. New York: W. W. Norton & Company.

[2] Valentine, J. W. (2004). *On the Origin of Phyla*. Chicago: University of Chicago Press.

[3] Foote, M. (1997). The evolution of morphological diversity. *Annual Review of Ecology and Systematics*, 28, 129–152.

[4] Erwin, D. H. (2007). Disparity: morphological pattern and developmental context. *Palaeontology*, 50(1), 57–73.

[5] Waddington, C. H. (1942). Canalization of development and the inheritance of acquired characters. *Nature*, 150, 563–565.

[6] Davidson, E. H., & Erwin, D. H. (2006). Gene regulatory networks and the evolution of animal body plans. *Science*, 311(5762), 796–800.

[7] Moran, N. A. (2002). Microbial minimalism: genome reduction in bacterial pathogens. *Cell*, 108(5), 583–586.

[8] McCutcheon, J. P., & Moran, N. A. (2012). Extreme genome reduction in symbiotic bacteria. *Nature Reviews Microbiology*, 10(1), 13–26.

[9] Force, A., Lynch, M., Pickett, F. B., Amores, A., Yan, Y. L., & Postlethwait, J. (1999). Preservation of duplicate genes by complementary, degenerative mutations. *Genetics*, 151(4), 1531–1545.

[10] Wagner, A. (2005). *Robustness and Evolvability in Living Systems*. Princeton, NJ: Princeton University Press.

[11] Wagner, A. (2008). Robustness and evolvability: a paradox resolved. *Proceedings of the Royal Society B: Biological Sciences*, 275(1630), 91–100.

[12] Haddad, W. M., Chellaboina, V., & Nersesov, S. G. (2006). *Impulsive and Hybrid Dynamical Systems: Stability, Dissipativity, and Control*. Princeton, NJ: Princeton University Press.

[13] Raup, D. M., & Sepkoski, J. J. (1982). Mass extinctions in the marine fossil record. *Science*, 215(4539), 1501–1503.

[14] Jablonski, D. (1986). Background and mass extinctions: the alternation of macroevolutionary regimes. *Science*, 231(4734), 129–133.

[15] Hughes, M., Gerber, S., & Wills, M. A. (2013). Clades reach highest morphological disparity early in their evolution. *Proceedings of the National Academy of Sciences*, 110(34), 13875–13879.

[16] Blount, Z. D., Lenski, R. E., & Losos, J. B. (2018). Contingency and determinism in evolution: Replaying life's tape. *Science*, 362(6415), eaam5979.

[17] Popper, K. (1959). *The Logic of Scientific Discovery.* London: Hutchinson & Co.

[18] Jeffery, W. R. (2009). Regressive evolution in Astyanax cavefish. *Annual Review of Genetics*, 43, 25–47.

[19] Galis, F. (1999). Why do almost all mammals have seven cervical vertebrae? Developmental constraints, Hox genes, and cancer. *Journal of Experimental Zoology*, 285(1), 19–26.

[20] Maynard Smith, J., Burian, R., Kauffman, S., Alberch, P., Campbell, J., Goodwin, B., Lande, R., Raup, D., & Wolpert, L. (1985). Developmental constraints and evolution. *Quarterly Review of Biology*, 60(3), 265–287.

[21] Gould, S. J. (1970). Dollo on Dollo's law: irreversibility and the status of evolutionary laws. *Journal of the History of Biology*, 3(2), 189–212.

[22] Collin, R., & Miglietta, M. P. (2008). Reversing opinions on Dollo's Law. *Trends in Ecology & Evolution*, 23(11), 602–609.

[23] Schluter, D. (2000). *The Ecology of Adaptive Radiation.* Oxford: Oxford University Press.

[24] Smithwick, F. M., & Stubbs, T. L. (2018). Phanerozoic survivors: Actinopterygian evolution through the Permo-Triassic and Triassic-Jurassic mass extinction events. *Evolution*, 72(2), 348–362. Data: Dryad 10.5061/dryad.3vs6b.

[25] Bazzi, M., Kear, B. P., Blom, H., Ahlberg, P. E., & Campione, N. E. (2018). Static dental disparity and morphological turnover in sharks across the end-Cretaceous mass extinction. *Current Biology*, 28(16), 2607–2615. Data: Dryad 10.5061/dryad.k30c2n0.

[26] Sclafani, J. A., Congreve, C. R., Krug, A. Z., & Patzkowsky, M. E. (2018). Effects of mass extinction and recovery dynamics on long-term evolutionary trends: a morphological study of Strophomenida (Brachiopoda) across the Late Ordovician mass extinction. *Paleobiology*, 44(4), 603–619. Data: Dryad 10.5061/dryad.4bp82rc.

[27] Szklarczyk, D., et al. (2023). The STRING database in 2023: protein–protein association networks and functional enrichment analyses for any sequenced genome of interest. *Nucleic Acids Research*, 51(D1), D638–D646.

[28] Chatr-Aryamontri, A., et al. (2017). The BioGRID interaction database: 2017 update. *Nucleic Acids Research*, 45(D1), D369–D379.